Escherichia coli SecA shape and dimensions

Brian Shilton[a], Dmitri I. Svergun[b,c], Vladimir V. Volkov[c], Michel H.J. Koch[b], Stephen Cusack[d], Anastassios Economou[a,*]

[a]*Institute of Molecular Biology and Biotechnology and Department of Biology, University of Crete, P.O. Box 1527, GR-711 10 Iraklio, Crete, Greece*
[b]*European Molecular Biology Laboratory, Hamburg Outstation, Notkestraße 85, D-22603 Hamburg, Germany*
[c]*Institute of Crystallography, Russian Academy of Sciences, Leninsky pr. 59, 117333 Moscow, Russia*
[d]*European Molecular Biology Laboratory, Grenoble Outstation, c/o ILL, Avenue des Martyrs, B.P. 156, 38042 Grenoble Cedex 9, France*

Received 22 July 1998; revised version received 3 September 1998

Abstract SecA shape and conformational flexibility in solution were studied by small angle X-ray scattering. Dimeric SecA is a very elongated molecule, 15 nm long and 8 nm wide. SecA is therefore four times as long as the membrane is wide. The two globular protomers are distinctly separated and share limited surface of intermolecular contacts. ATP, ADP or adenylyl-imidodiphosphate (AMP-PNP) binding does not alter the SecA radius of gyration. A SecA mutant that catalyzes multiple rounds of ATP hydrolysis does not undergo conformational changes detectable by small angle X-ray scattering (SAXS). We conclude that SecA conformational alterations observed biochemically during nucleotide interaction are only small-scale and localized. The ramifications of these findings on SecA/SecYEG interaction are discussed.

Key words: SecA; Translocase; Small angle X-ray scattering; SecYEG; Preprotein translocation

1. Introduction

Trafficking of polypeptides across biological membranes is catalyzed by complex molecular machines, termed preprotein translocases or translocons [1]. The core of bacterial translocase is a complex of the trimeric membrane protein SecYEG with the peripheral ATPase SecA [2–5]. SecA is a homodimer [6–8] and can be dissected into two proteolytic fragments, thought to represent the primary structural elements [9]: the N-terminal domain (N-domain; residues 1–609) comprising the high affinity nucleotide binding site NBD1 [9,10] and the C-terminal domain (C-domain; residues 610–901) that interacts with SecY [11,12] and promotes dimerization [8]. Both domains can acquire an integral membrane topology [13–15].

Preproteins bind to translocase at SecA [2,3] and trigger multiple rounds of ATP binding and hydrolysis at NBD1. As a result, SecA interchanges between a membrane integral and a more peripheral state at SecYEG [11,16], thus allowing translocase to move processively along the polymeric substrate [3]. Translocase dissociates from the preprotein only after its whole chain length has been transported to the periplasm, where it is fully released. SecA cycling is essential for translocation [16]. However, the molecular mechanism by which SecA catalyzes substrate vectorial movement is completely unknown. One hypothesis is that preprotein domains are physically transported by SecA during its own membrane insertion [11,16]. The nature and extent of SecA conformational changes at SecYEG and membrane topology, both essential elements of the above model, have been poorly characterized using only indirect biochemical approaches such as proteolysis [11,14,16,17] and modification of cysteinyl residues [14,17]. Translocase structure at atomic resolution remains unknown.

Cytosolic SecA is an essential intermediate of SecA membrane cycling [15] and is more amenable to structural analysis than the integral membrane form. We have now characterized soluble SecA by employing small angle X-ray scattering (SAXS). New computational techniques allow low resolution shape determination from SAXS data [18,19]. Moreover, SAXS is a direct tool to study conformational changes taking place in soluble enzymes under native conditions since it provides accurate information on changes in the radius of gyration [20]. SAXS has been successfully used to study chaperone/polypeptide substrate interactions [21,22]. We have determined that SecA has an unusually elongated shape. Moreover, SecA does not undergo any large-scale conformational changes upon binding or hydrolysis of ATP in solution.

2. Materials and methods

2.1. Bacterial strains and biochemicals

Growth of *Escherichia coli* BL21.19 (*secA13[Am]*, *supF[Ts]*, *trp(Am)*, *zch::Tn10*, *recA::cat*) carrying plasmids pZ52SecA, pT109N-SecA, pD209N-SecA and pR509K-SecA, and SecA purification were as described [10,16]. Nucleotides and trypsin were from Boehringer Mannheim and chromatography resins from Pharmacia.

2.2. Small angle X-ray scattering and data treatment

All measurements (wavelength of $\lambda = 0.15$ nm; beamline X33; at 15°C) [23] were made at the European Molecular Biology Laboratory Outstation at the Deutsches Elektronen-Synchrotron (Hamburg, Germany). Data were collected on a quadrant multiwire proportional detector with delay line readout. The sample-detector distances of 1.4 m (low angles), 2.8 and 3.4 m (higher angles) were measured to cover the range of momentum transfer $0.2 < s < 5.0$ nm^{-1} ($s = 4\pi \sin\theta/\lambda$, where 2θ is the scattering angle). Twenty successive 30-s exposures were recorded for each sample; there was no evidence of protein degradation over this time interval. Averaging of frames, corrections for detector response and beam intensity and buffer subtraction were done using the programs SAPOKO (D.I.S. and M.H.J.K, unpublished) and OTOKO [24]. SecA preparations were >98% pure and monodisperse as evidenced by native polyacrylamide gel electrophoresis and size exclusion chromatography (data not shown). Protein samples were dialyzed against 20 mM Tris-HCl, pH 7.6, 1 mM DTT, containing 20 mM NaCl and 5 mM $MgCl_2$; nucleotides were added to the protein sample (80 μl) and its matching dialysis buffer just prior to the measurements. Protein concentrations were 3–5 mg/ml (2.8 m and 3.4 m camera lengths) and 15 mg/ml (1.4 m camera length); no noticeable concentration effect was observed for concen-

*Corresponding author. Fax: (30) (81) 39 11 66.
E-mail: aeconomou@imbb.forth.gr

Abbreviations: SAXS, small angle X-ray scattering; AMP-PNP, adenylyl-imidodiphosphate

PII: S0014-5793(98)01141-7

trations up to 7 mg/ml. To avoid systematic errors, the same preparation of wild-type SecA was used with identical camera settings. Maximum dimension of the SecA particle was estimated from the difference curves using the orthogonal expansion program ORTOGNOM [25]. The distance distribution function $P(r)$ was evaluated by the indirect transform package GNOM [26,27]. These data also yield the forward scattering $I(0)$, which is proportional to the molecular weight of the solute, and the radius of gyration (R_g) of the particle.

2.3. SecA shape determination

For the ab initio shape determination, the envelope of the particle is represented by an angular border function $F(\omega)$, where $(\omega) = (\theta,\varphi)$ are spherical coordinates, which is parameterized as:

$$F(\omega) = \sum_{l=0}^{L} \sum_{m=-l}^{l} f_{lm} Y_{lm} (= Л3 > \omega) \quad (1)$$

where f_{lm} are complex numbers and $Y_{lm}(\omega)$ spherical harmonics. The resolution of this representation is $\delta r = (5/3)^{1/2}\pi R_g/(L+1)$, and the number of parameters for a general case $(L+1)^2$. The non-linear minimization program SASHA [19,28] employs the algorithms to rapidly compute the scattering intensities $I(s)$ from such a model [18,28]. The program starts from a spherical initial approximation and determines the coefficients f_{lm} by minimizing the R-factor

$$R_I^2 = \frac{\sum_{j=1}^{N} \{W(s_j[I(s_j) - I_{exp}(s_j)]\}^2}{\sum_{j=1}^{N} [W(s_j) I_{exp}(s_j)]^2} \quad (2)$$

where N is the number of experimental points and the weighting function is $W(s_j) = s_j^2/[\sigma((s_j)/I_{exp}(s_j)]$, where $I_{exp}(s_j)$ and $\sigma(s_j)$ are the experimental intensity and its standard deviation, in the j-th point, respectively. As the scattering from intraparticle inhomogeneities dominates the outer part of the scattering curve, only data up to $s = 2.5$ nm^{-1} were used for the shape determination. Moreover, a constant term was subtracted from the data to force the intensity decrease as s^{-4} at higher angles ($s > 1.5$ nm^{-1}) in accordance with Porod's law for homogeneous bodies [29].

SecA is a homodimer [6–8] and it is logical to assume that it possesses a twofold symmetry axis. Imposing this symmetry restriction on the envelope function describing the entire dimeric particle, all f_{lm} coefficients with odd m vanish in Eq. 1 which reduces the number of free parameters for a given L. Alternatively, $F(\omega)$ can represent the shape of the monomer, and the scattering amplitude from the symmetry-related monomer is generated to yield the intensity from the dimer [30]. This approach enhances the resolution by parameterizing the shape of a monomer rather than that of a dimer, adding only the distance between monomers as an additional parameter.

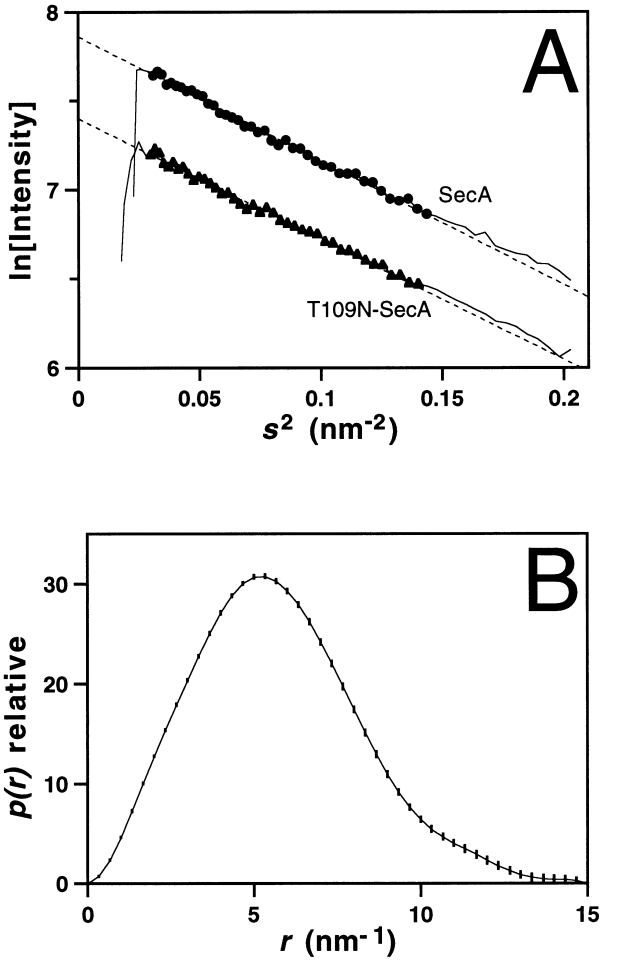

Fig. 1. Analysis of small angle X-ray scattering data used to determine SecA R_g and dimensions. A: Guinier curves for soluble, unliganded SecA. Data were recorded at a sample-detector distance of 2.8 m (SecA; ●) and 3.4 m (T109N-SecA; ▲). Solid curves represent the complete data set. The symbols indicate those data points used for calculation of a linear least-squares fit which is indicated by the broken lines. B: Distance distribution function of SecA evaluated from the experimental data using the program GNOM [26,27].

3. Results

3.1. Radius of gyration and maximal dimension of the SecA molecule

SecA was exposed to synchrotron radiation and scattering data were collected. Data from low angle settings were used to determine the radius of gyration (R_g). Guinier plots (ln $I(s)$ vs. s^2) for the SecA protein were linear at the low angle end (s^2 from 0.04 to 0.16 nm^{-2}), and deviate gradually from a least-squares line at higher angles ($s^2 > 0.2$ nm^{-2}) indicating that the protein was monodisperse (Fig. 1A). The maximum dimension (D_{max}) of the particle was found to be 15.0 ± 0.5 nm (see Section 2). The scattering at 0 angle (forward scattering; $I(0)$) is coincident with the direct beam and is proportional to the molecular weight of the scattering molecule. The $I(0)$ values determined for bovine serum albumin (1110 at 3.8 mg/ml) and for SecA (1890 at 2.2 mg/ml), yield a 200-kDa molecular weight for SecA, consistent with soluble SecA being homodimeric [6–8]. Using the length distribution function $P(r)$

Table 1
Radius of gyration of SecA

Protein	Radius of gyration (nm)			
	–	ADP	ATP	AMP-PNP
SecA	**4.52** (4.49, 4.54)	**4.47** (4.42, 4.51)	**4.48** (4.47, 4.53, 4.47, 4.44)	**4.47** (4.48, 4.46)
T109N-SecA	**4.39** (4.40, 4.38)	**4.45** (4.42, 4.50, 4.42)	**4.45** (4.46, 4.41, 4.48)	**4.41** (4.38, 4.43)

The R_g values were calculated from distance distribution functions, obtained using the indirect transform method, as implemented in the program GNOM [26,27,47]. Values in parentheses are individual determinations; bold face values represent the average of individual determinations.

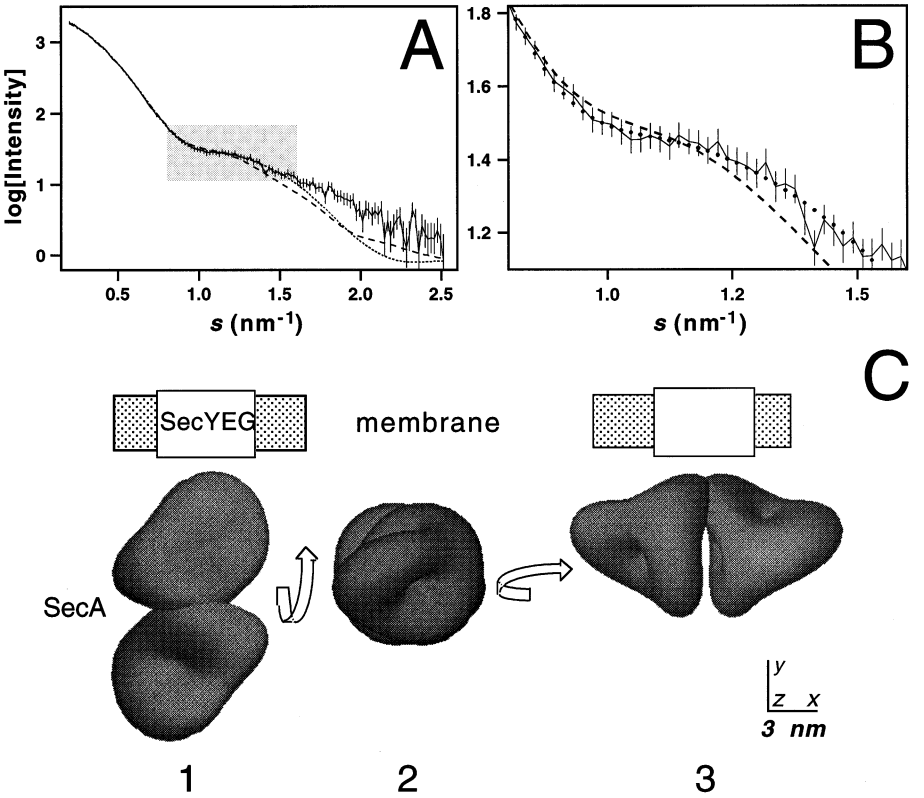

Fig. 2. Determination of SecA shape in solution. A: Experimental scattering curve showing the fit of the data used to construct the SecA shape models. The curve of the mathematical fit using a single dimeric shape model at $L=4$ (dashed lines) and the curve calculated from the restored two-monomer model at $L=3$ (dotted lines; presented in panel C below) were superimposed on the curve of the experimental data from SecA solution scattering (solid line with error bars). B: The shaded area between s values of 0.8 and 1.6 nm^{-1} of plot A has been enlarged to allow better comparison of the curves. C: Low resolution shape model of the SecA molecule consisting of two monomers. SecA is calculated to be an elongated particle with approximate maximal dimensions 15×8 nm. The best-fitting shape model for SecA is shown from three different view points (views 1–3). View 1: the twofold axis coincides with the Z axis (normal to the plane of the paper), the two monomers are separated along the Y axis; a rotation of 90° about the X axis produces view 2 where the twofold axis coincides with Y and the two monomers are separated along Z; view 3 is view 2 rotated 90° around Y so that the twofold axis coincides with Y and the two monomers are separated along Z. In all three views the orientation of SecA relative to the membrane plane is hypothetical. SecA could also be positioned parallel to the membrane if the shape in view 3 is rotated along Z by 180° (not shown). For comparison of relative sizes, schematic representations of a lipid bilayer membrane (shaded rectangle; thickness of 3.4–4 nm [43,44] encompassing a hydrophobic core of ∼3 nm [44]) and of a SecYEG trimer (white rectangle) are also shown, drawn to scale. SecYEG diameter was estimated from the crystallographically determined dimensions of membrane proteins, such as the potassium channel from *Escherichia coli* [44] and the photosystem I from *Synechococcus* [45]. Each transmembrane helix in these proteins occupies ∼2.7 nm^2 [43–46]. SecYEG (with a stoichiometry of 1:1:1) is predicted to contain 15 membrane-spanning α-helices [2]. Tightly packed SecYEG would occupy an area of ∼40 nm^2, corresponding to a diameter of ∼7 nm.

(Fig. 1B), which analyzes the distribution of distances between pairs of points in a particle [26], its radius of gyration (R_g) was determined to be 4.47 ± 0.06 nm. Similar values were obtained for the point mutants T109N-SecA (Table 1, see below), D209N-SecA and R509K-SecA (data not shown). The distance distribution function is not symmetric around the calculated R_g of ∼4.5 nm (Fig. 1B). If SecA were a globular protein, the $P(r)$ function would be expected to be 0 beyond approximately 11 nm. Instead, the calculated distribution displays significant values up to 15 nm. We conclude that SecA is an unusually elongated molecule.

3.2. Shape of the SecA dimer

The shape of the SecA particle was determined using data from the high angle setting. The resolution of the shape is determined by the parameter L (see Eqs. 1 and 2, Section 2) and depends on the information content in the scattering data. The latter is related to the number of the Shannon channels (N_s) covered by the experimental range, $N_s = D_{max}s_{max}/\pi$ [31,32]. Low resolution shape determination provides an unambiguous solution if the number of independent parameters in the model does not exceed 1.5 N_s [20]. Our data with a value $N_s = 12$ should allow us to perform the shape determination of the entire dimer with $L=4$ or 5 (13 and 18 free parameters, respectively). However, attempts to fit the scattering data using a single shape representation failed at this level of resolution. A typical best fit at $L=4$ yields $R_I = 2.2\%$ and displays systematic deviations from the experimental data starting from the onset of the first shoulder (Fig. 2A,B). The obtained shapes contained artificially enhanced contributions from higher harmonics (not shown) presumably due to the elongated nature of SecA.

Taking an alternative approach, we represented the low resolution structure of SecA in terms of the shape of its monomeric part (see Section 2; [30]). At the multipole resolution $L=3$, the number of independent parameters (shape coefficients plus the distance Δd between the monomers) was 15 (the reduction by two parameters is due to arbitrary shifts

of the dimer along the twofold axis and its rotation around this axis). The restored structure at a spatial resolution of 3.3 nm is presented in Fig. 2C and yields an excellent fit to the experimental data, with $R_I = 1.5\%$ (Fig. 2A,B). The solution is stable to the initial approximation and also to the initial choice of Δd. Several minimization runs yielded the monomer shapes and arrangements similar to those presented in Fig. 2C (views 1–3) yielding the radius of gyration of the monomer $R_{gm} = 3.3 \pm 0.1$ nm and the separation of the centres of mass of the monomers $\Delta d = 5.9 \pm 0.3$ nm. The maximum width of the molecule along its short axis was calculated to be 8 nm (Fig. 2C, view 2). The shape representation in Fig. 2C illustrates the anisometric nature of the SecA particle. The two protomers appear to be relatively globular and are distinctly separated from each other. A single low resolution angular envelope function centered in the middle of the homodimer cannot provide an adequate description of the entire shape, thus explaining the poor fit obtained for the single shape approximation (Fig. 2A,B).

3.3. Effect of nucleotides on SecA conformation studied by SAXS

SecA binds ATP and ADP in solution with high affinity in the absence of any other ligands [33–36]. Using proteolysis and tryptophan fluorescence, nucleotide binding was shown to affect SecA conformation [34–36]. However, these indirect approaches cannot provide a true measure of the scale of the conformational change. To determine the extent of SecA physical flexibility during nucleotide interaction we examined the effect of nucleotides on SecA shape directly, by SAXS. SecA scattering data were collected in the presence of three nucleotides (ATP, ADP and AMP-PNP) known to affect SecA conformation in solution and at the membrane [4,11,14,16,34,35]. R_g values for SecA in the presence or absence of nucleotides were similar (Table 1). To exclude the possibility that this result was due to reduced sensitivity of the experimental method, we extended our data collection to an s value of 5 nm^{-1}. Scattering at higher angles is more sensitive to structural changes and the higher protein concentrations used result in better signal-to-noise ratios. However, even under these conditions, there is no detectable nucleotide-dependent conformational change in SecA (Fig. 3). We ruled out the possibility of an inherent problem in our SecA preparations since under the same experimental conditions used for the SAXS experiments we could demonstrate changes in the trypsinolysis profile caused by the binding of ADP (S. Karamanou, E. Vrontou, G. Sianidis and A.E., manuscript in preparation) as described previously [36]. Finally, since the ADP conformation of SecA is very stable ([36], S. Karamanou and A.E., unpublished results) it is unlikely that the nucleotide-induced conformations are too short-lived to be detected by SAXS.

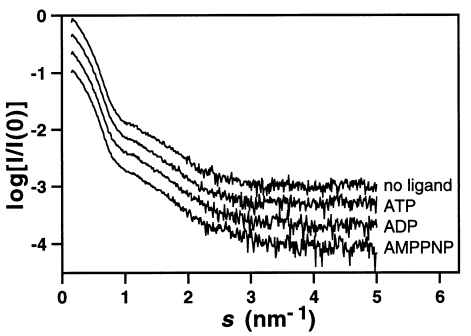

Fig. 3. SAXS analysis of nucleotide-SecA interaction. The curves represent data measured at two sample-detector distances and two protein concentrations. Scattering from SecA at a concentration of 4 mg/ml was measured at 2.8 m (low angle) and merged with data recorded using a 1.4-m camera length and a protein concentration of 15 mg/ml. The program MERGER (M.H.J.K., unpublished) was used to match the two curves in the region from $s = 0.502$ to $s = 0.628$ nm^{-1}. The $I(0)$ values have been altered so that the curves are separated sufficiently for comparison. The curves are superimposable except at the higher angle end, which is relatively noisy and sensitive to errors in buffer subtraction. SecA was in 20 mM Tris-Cl, pH = 7.6, 20 mM NaCl and 5mM $MgCl_2$; nucleotides were present at a concentration of 2 mM.

Could it be that multiple rounds of ATP hydrolysis, more closely resembling SecA engaged in translocation, are required for substantial conformational changes to occur? In contrast to the basal ATPase activity of soluble SecA, translocation ATPase activity (observed in the presence of membranes and preprotein) is high level [2,33]. We tested the requirement for ATP hydrolysis by employing T109N-SecA, a mutant which is translocation competent ([10], A.E., unpublished results) but has a basal ATPase activity increased severalfold over that of wild-type SecA [10]. T109N-SecA displays similar R_g values in the presence or absence of ATP (Table 1) indicating that SecA shape remains largely unaltered. We conclude that the nucleotide-induced conformational changes in soluble SecA observed by proteolysis and indirect fluorescence are small and localized.

4. Discussion

We have measured the small-angle X-ray scattering of SecA and determined the low resolution structure of the SecA dimer in solution. To our knowledge, this is the first determination of SecA shape and dimensions. Furthermore, independently of any previous model, we demonstrated that SecA does not undergo any major shape alteration upon interaction with nucleotides. These results give rise to a number of testable hypotheses and necessitate an evolution of current models of the molecular mechanism of SecA membrane cycling [2,11], the extent of SecA periplasmic exposure and flexibility of SecA domains [2] and the physical dimensions and shape of SecA/SecYEG complexes [13].

The SecA particle is very elongated, 15 nm long and 8 nm wide (Fig. 2C). The dimer is organized in two independent and distinctly separated spheres with a limited surface of interaction between the protomers. The structural isolation of the protomers suggests that the two primary N- and C-domains of SecA lie in close proximity in three-dimensional space. This would explain why both domains are found to be membrane-inserted [13,14] and why regions of the C-domain are important for ATP binding to the N-domain [8,34]. The model presented here fits almost perfectly to the experimental data suggesting a unique and rigid dimeric SecA shape in solution (Fig. 2C). Nevertheless, it cannot be excluded that our model represents an 'average' structure out of a set of different conformations of the protein. Furthermore, in building the model it was assumed that the protomers are symmetrical but slight differences in the structure of each protomer are possible. These questions will be resolved when a high resolution structure becomes available.

E. coli SecA has proven recalcitrant to structure elucidation by conventional crystallography [37]. In contrast, SAXS has provided us with a rapid and powerful method to determine SecA structure, albeit at low resolution. A low resolution electron microscopy analysis of thin-sectioned SecA crystals has been presented, but the projection images of the crystal were not sufficient to determine SecA shape [37]. A 'dumbbell' shape, apparent in one of the projections, was interpreted as two SecA dimers forming tetramers or octamers in the crystal lattice. Both the small size (12 nm) and the pattern of electron density of the proposed SecA dimer do not match our model of soluble SecA. Furthermore, in agreement with biochemical measurements [6–8], in all our SAXS experiments, only a dimeric form of soluble SecA was detected even at high protein concentrations. It may be that the orientation of SecA in the three-dimensional crystals is such that the particle shape is not evident when viewed in projection.

How does SecA associate with SecYEG? Given its elongated shape, membrane-inserted SecA could acquire either one of two possible orientations: one perpendicular and one parallel to the membrane plane (Fig. 2C, views 1–3). In the former (view 1), only one pole of the dimer (e.g. one of the two protomers) would be expected to insert. In the latter orientation (view 3), central parts of the dimer, consisting of regions from both protomers, would insert. In either case, intermolecular asymmetry, which is expected to be important for enzymatic processivity [3], can be established. Available data, obtained using proteolysis [11,13,15,17,38,39] and accessibility to sulfhydryl-reacting reagents [14,17], cannot discriminate between the two topologies. During SecA association with the significantly smaller SecYEG trimer (Fig. 2C), the sheer size of SecA (almost four times the membrane thickness; see Fig. 2C) is bound to sterically influence translocase shape and stoichiometry. SecA membrane-inserted at SecYEG is not laterally accessible to labeling from the lipid phase [40,41], suggesting that membrane-embedded domains of SecA may be largely shielded from phospholipids by SecYEG. A single SecYEG trimer may be too small to envelop the gargantuan SecA molecule. Alternatively, as was proposed for its eucaryotic homologue Sec61 [42], bacterial translocase may comprise several SecYEG trimers.

SAXS provides a direct measure of protein conformational dynamics. Our results indicate that the overall shape of SecA remains unaltered when it interacts with ATP or ADP (Fig. 3 and Table 1). Conformational changes during soluble SecA-nucleotide interaction have been inferred from changes in proteolytic susceptibility and tryptophan fluorescence [15,35,36,38]. We too have detected ADP-induced changes in SecA using trypsinolysis (S. Karamanou, E. Vrontou, G. Sianidis and A.E., manuscript in preparation). However, as documented previously, this change is localized to a trypsin-sensitive loop in the middle of the sequence [36]. We conclude that nucleotide binding to soluble SecA does not cause significant motions of large domains or of whole protomers which would be detectable by SAXS [20] but rather only limited, localized structural alterations. SecA shape and dimensions determined by SAXS provide the first baseline against which all other conformational changes can now be measured in a quantitative manner.

How flexible is the 15×8-nm SecA particle in the membrane plane during translocation? Binding of SecY, lipid and preprotein may promote low energy states of SecA. An important element of SecA-mediated translocation was proposed to be a substantial conformational change leading to membrane insertion of the 30-kDa C-domain [11,16]. However, recent experiments suggest that the C-domain of SecA may not insert in the membrane independently of the N-domain [13] and, moreover, the organization of soluble and membrane-bound SecA appears to be similar [9,12,14,15]. It cannot be excluded that movement of the N- and C-domains of SecA relative to each other during translocation is less dramatic than was originally suggested by proteolysis [11]. An attractive alternative mechanism suggested by the SecA shape (Fig. 2C) could involve rotational movement of the two protomers. SAXS is not appropriate to resolve these issues since SecA scattering cannot be deconvoluted from that of lipids, membrane subunits of translocase and preprotein. To elucidate SecA membrane topology, conformations and SecYEG interactions, additional quantitative biophysical methods will be required.

Acknowledgements: We thank B. Pozidis for help with chromatography, L. Karamanou for several useful discussions and for gifts of purified proteins, A. Kuhn for reading the manuscript, D. Dialektakis (Minotech) for bacterial fermentation and D. Oliver for gifts of SecA mutant derivatives. This work was supported by grants from the Greek Secretariat of Research and Technology (No. GSRT-5775 to A.E.), INTAS (No. 96-1115 to M.H.J.K. and D.I.S.) and the European Union (the HCMP Access to Large Installations Project for Small Angle X-ray Scattering Work at EMBL, Hamburg, No. CHGE-CT93-0040; TMR-ERBFMRXCT960035 to A.E. and S.C.; BIOTECH2-BIO4-CT97-2143 to D.I.S.). B.S. is a European Molecular Biology Organization and Human Frontiers of Science Program postdoctoral fellow and V.V.V. an EMBL research fellow.

References

[1] Schatz, G. and Dobberstein, B. (1994) Science 271, 1519–1526.
[2] Wickner, W. and Leonard, M. (1996) J. Biol. Chem. 271, 29514–29516.
[3] Economou, A. (1998) Mol. Microbiol. 27, 511–518.
[4] Matsumoto, G., Yoshihisa, T. and Ito, K. (1997) EMBO J. 16, 6384–6393.
[5] Manting, E.H., Van der Does, C. and Driessen, A.J.M. (1997) J. Bacteriol. 179, 5699–5704.
[6] Akita, M., Shinkai, A., Matsuyama, S. and Mizushima, S. (1991) Biochem. Biophys. Res. Commun. 174, 211–216.
[7] Driessen, A.J. (1993) Biochemistry 32, 13190–13197.
[8] Hirano, M., Matsuyama, S. and Tokuda, H. (1996) Biochem. Biophys. Res. Commun. 229, 90–95.
[9] Price, A., Economou, A., Duong, F. and Wickner, W. (1996) J. Biol.Chem. 271, 31580–31584.
[10] Mitchell, C. and Oliver, D. (1993) Mol. Microbiol. 10, 483–497.
[11] Economou, A. and Wickner, W. (1994) Cell 78, 835–843.
[12] Snyders, S., Ramamurthy, V. and Oliver, D. (1997) J. Biol. Chem. 272, 11302–11306.
[13] Eichler, J. and Wickner, W. (1997) Proc. Natl. Acad. Sci. USA 94, 5574–5581.
[14] Ramamurthy, V. and Oliver, D.B. (1997) J. Biol. Chem. 272, 23239–23246.
[15] Chen, X., Brown, T. and Tai, P.C. (1998) J. Bacteriol. 180, 527–537.
[16] Economou, A., Pogliano, J.P., Beckwith, J., Oliver, D.B. and Wickner, W. (1995) Cell 83, 1171–1181.
[17] Kim, Y.J., Rajapandi, T. and Oliver, D.B. (1994) Cell 78, 845–853.
[18] Svergun, D.I. and Stuhrmann, H.B. (1991) Acta Crystallogr. A47, 736–744.
[19] Svergun, D.I., Volkov, V.V., Kozin, M.B. and Stuhrmann, H.B. (1996) Acta Crystallogr. A52, 419–426.
[20] Durchschlag, H., Zipper, P., Wilfing, R. and Purr, G. (1991) J. Appl. Crystallogr. 24, 822–831.

[21] Shi, L., Kataoka, M. and Fink, A.L. (1996) Biochemistry 35, 3297–3308.
[22] Wilbanks, S.M., Chen, L., Tsuruta, H., Hodgson, K.O. and McKay, D.B. (1995) Biochemistry 34, 12095–12106.
[23] Koch, M.H.J. and Bordas, J. (1983) Nucl. Instrum. Methods 208, 461–469.
[24] Boulin, C., Kempf, R., Koch, M.H.J. and McLaughlin, S. (1986) Nucl. Instrum. Methods A249, 399–407.
[25] Svergun, D.I. (1993) J. Appl. Crystallogr. 26, 258–267.
[26] Svergun, D.I., Semenyuk, A.V. and Feigin, L.A. (1988) Acta Crystallogr. A44, 244–250.
[27] Svergun, D.I. (1992) J. Appl. Crystallogr. 25, 495–503.
[28] Svergun, D.I. (1997) J. Appl. Crystallogr. 30, 792–797.
[29] Feigin, L.A. and Svergun, D.I. (1987) Structure analysis by small-angle X-ray and neutron scattering, Plenum Press, New York, NY.
[30] Svergun, D.I., Volkov, V.V., Kozin, M.B., Stuhrmann, H.B., Barberato, C. and Koch, M.H.J. (1997) J. Appl. Crystallogr. 30, 798–802.
[31] Shannon, C.E. and Weaver, W. (1949) The Mathematical Theory of Communication, University of Illinois Press, Urbana, IL.
[32] Moore, P.B. (1980) J. Appl. Crystallogr. 13, 168–175.
[33] Lill, R., Cunningham, K., Brundage, L., Ito, K., Oliver, D. and Wickner, W. (1989) EMBO J. 8, 961–966.
[34] Matsuyama, S., Kimura, E. and Mizushima, S. (1990) J. Biol. Chem. 265, 8760–8765.
[35] Shinkai, A., Mei, L.H., Tokuda, H. and Mizushima, S. (1991) J. Biol. Chem. 266, 5827–5833.
[36] den Blaauwen, T., Fekkes, P., de Wit, J.G., Kuiper, W. and Driessen, A.J.M. (1996) Biochemistry 35, 11194–12004.
[37] Weaver, A.J., McDowall, A.W., Oliver, D.B. and Deisenhofer, J. (1992) J. Struct. Biol. 109, 87–96.
[38] Ulbrandt, N.D., London, E. and Oliver, D.B. (1992) J. Biol. Chem. 267, 15184–15192.
[39] van der Does, C., den Blaauwen, T., de Wit, J.G., Manting, E.H., Groot, N.A., Fekkes, P. and Driessen, A.J. (1996) Mol. Microbiol. 22, 619–629.
[40] Eichler, J., Brunner, J. and Wickner, W. (1997) EMBO J. 16, 2188–2196.
[41] Van Voorts, F., van der Does, C., Brunner, J., Driessen, A.J.M. and de Kruijff, B. (1998) Biochemistry, in press.
[42] Hanein, D., Matlack, K.E., Jungnickel, B., Plath, K., Kalies, K.U., Miller, K.R., Rapoport, T.A. and Akey, C.W. (1996) Cell 87, 721–732.
[43] Yeats, T.O., Komiya, H., Rees, D.C., Allen, J.P. and Feher, G. (1987) Proc. Natl. Acad. Sci. USA 84, 6438–6442.
[44] Doyle, D.A., Cabral, J.M., Pfuetzner, R.A., Kuo, A., Gulbis, J.M., Cohen, S.L., Chait, B.T. and MacKinnon, R. (1998) Science 280, 69–77.
[45] Michel, H. and Desenhofer, J. (1990) Current Topics in Membranes and Transport, Vol. 36, pp. 53–69, Academic Press.
[46] Krauss, N., Hinrichs, W., Witt, I., Fromme, P., Pritzkow, W., Dauter, Z., Betzel, C., Wilson, K.S., Witt, H.T. and Saenger, W. (1993) Nature 361, 326–331.
[47] Semenyuk, A.V. and Svergun, D.I. (1991) J. Appl. Crystallogr. 24, 537–540.